JOURNAL OF MATERIALS SCIENCE **30** (1995) 1931–1938

Preparation and properties evaluation of zirconia-based/Al_2O_3 composites as electrolytes for solid oxide fuel cell systems

Part I *Powder preparation and characterization*

L. M. NAVARRO, P. RECIO, P. DURÁN
Instituto de Cerámica y Vidrio (CSIC), Electroceramics Department 28500 Arganda del Rey, Madrid, Spain

The powder morphology and particle size of both mixtures of ultrafine yttria-doped zirconia (3 to 8 mol % Y_2O_3) and aluminium hydroxide (0 to 20 wt % Al_2O_3), and zirconia/yttria/alumina coprecipitated powders were studied using measurements of surface area, X-ray diffraction, differential thermal analysis, infrared spectroscopy, scanning electron microscopy, and transmission electron microscopy. All the powders were calcined at 800 °C for 10 minutes. Both the growth of zirconia crystallites and its crystallization temperature were strongly influenced by the presence of alumina. The crystallite zirconia growth was inhibited and the zirconia crystallization temperature was increased. This behaviour has been assumed to be due to the formation of a polycondensed chain of the type Zr–O–Al–O–Y–O–Al–O–Zr in which the diffusion distances were considerably augmented.

1. Introduction

The first high temperature fuel cell with zirconia electrolyte was used by Bauer and Preis [1]; however, the development of solid oxide fuel cell (SOFC) technology was not started until the early sixties. Since that time a wide variety of ceramic materials have been studied for their use in SOFC systems and an excellent technical evolution has taken place in recent years.

The basic principles of operation of a solid oxide fuel cell are shown schematically in Fig. 1. The electrolyte has to be an oxygen ion conductor material at high temperatures (900–1000 °C), usually yttria stabilized zirconia or ceria–gadolinia solid solutions, and an advantage of these fuel cells is that direct power generation (energy conversion efficiency of about 65%) from fossil fuels with internal reforming is possible. On the other hand, a relatively fast electrode kinetics and not rate-controlling is ensured [2].

The main problem of this fuel cell type is the severe requirements that the electrolytes used have to satisfy, among others the following: (a) phase stability in both reducing and oxidizing atmospheres for long periods of time in service ($\geqslant 5000$ h); (b) high and stable electrical conductivity ($\geqslant 10^{-2}$ S.cm^{-1}) at the fuel cell operating temperature; (c) no mixed conductivity, i.e., the ion transference number must be unity; and (d) relatively high mechanical properties ($\sigma \geqslant 500$ MPa at room temperature and $K_{IC} \geqslant 3$MPa m$^{1/2}$). An excellent review of ceramic fuel cells has been made by Minh [3].

It is well known that ceramic materials formulated in the zirconia-rich region ($\leqslant 9$ mol % Y_2O_3) of the ZrO_2–Y_2O_3 system could be used for different applications [4]. For example, those zirconia ceramics containing less than 3 mol % Y_2O_3, having a tetragonal structure, are currently being applied for used as structural ceramics because of their high strength and fracture toughness, and constitute a ceramic materials family (Y-TZP) called toughened zirconia ceramics. However, owing to the metastability of the tetragonal zirconia solid solutions, Y-TZP ceramics present an ageing phenomenon below 550 °C accompanied by tetragonal to monoclinic phase transformation which results in a dramatic reduction of both their mechanical and electrical properties.

On the other hand, the tetragonal zirconia solid solution formation takes place by the substitution of Y^{3+} for Zr^{4+} in the zirconia lattice with the formation of oxygen vacancies. At high temperature an ionic conductivity is present by the mobility of oxygen ions between the vacancies in the defective zirconia lattice, and such a characteristic could be exploited in the use of these zirconia ceramics as electrolytes. In fact, they could be applied in oxygen sensors for fuel control in automobiles and in SOFC systems [5–7]. However, there are two main problems at present with this kind of electrolyte: on the one hand, its lower ionic conductivity than that of cubic stabilized zirconia [8] at the SOFC operating temperature (900–1000 °C) and, on the other, its very bad ageing behaviour. Even if it has extremely high mechanical properties, the above characteristics preclude its use as an electrolyte for SOFC systems [3].

Although zirconia ceramics containing between 3 and 6.5 mol % Y_2O_3 (Y-PSZ) presented both a better

0022–2461 © *1995 Chapman & Hall*

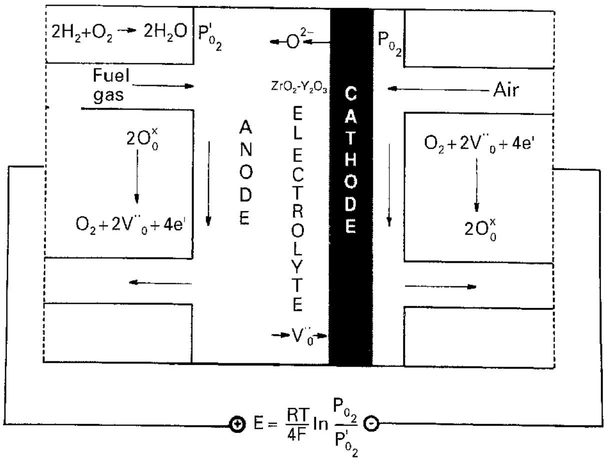

Figure 1 Schematic view of a solid oxide fuel cell (SOFC).

ageing behaviour and a higher ionic conductivity [9–10], these properties could be seriously affected by the characteristics and annealing behaviour of a dual (tetragonal + cubic) microstructure typical of these kinds of zirconia ceramics.

Fully stabilized zirconia (FSZ) with a cubic structure, containing between 6.5 and 9 mol % Y_2O_3, is the most attractive zirconia ceramic to be used as an electrolyte in SOFC systems due to its higher electrical properties. However, it must be noted that both the mechanical and thermal properties of these zirconia ceramics are not as good as desired, and many efforts are being made to optimize them. In that sense, the introduction of a second phase with thermomechanical properties different from those of the matrix has been widely used for the development of partially and fully stabilized zirconias with better electrical and mechanical properties [11–12].

In the present study 1-xZrO_2-xY_2O_3 (x = 3, 4, 6 and 8 mol %) and 1-xZrO_2-xY_2O_3yAl_2O_3 (y = 5, 10 and 20 wt %) powders were prepared by the coprecipitation method. The influence of alumina on the zirconia powder morphology, calcining temperature and particle size of the calcined powders was studied. A commercial zirconia powder with the same alumina additions was utilized as reference.

2. Experimental procedure

In the present experiments the required amounts of zirconium oxychloride ($ZrOCl_2 \cdot 8H_2O$), yttrium chloride ($YCl_3 \cdot 6H_2O$) and aluminium nitrate ($Al(NO_3)_3 \cdot 9H_2O$) were dissolved in ethanol. Then the alcoholic solution was uniformly mixed and stirred into diluted ammonia water, maintaining the pH between 9 and 11 during the coprecipitation process to ensure total cationic precipitation. The coprecipitated powders were thoroughly washed until the chloride disappeared, filtered, dried, calcined at 800 °C in air for 10 minutes, and attrition-milled with a zirconia ball for 2h in ethanol. Thus fine powders with compositions 3 mol % Y_2O_3-97 mol % ZrO_2 (Y-TZP), 4–6 mol % Y_2O_3-96-94 mol % ZrO_2 (Y-PSZ), and 8 mol % Y_2O_3-92 mol % ZrO_2 (YSZ), with or without 5 to 20 wt % Al_2O_3, were prepared. The schematic flow diagram for powder preparation is shown in Fig. 2. The samples will be denoted as follows: a zirconia sample containing 3 mol % Y_2O_3, Z-3Y, and 10 wt % Al_2O_3, Z-3Y/10A. In the same way, we have Z-8Y or with 10 wt % Al_2O_3, Z-8Y/10A.

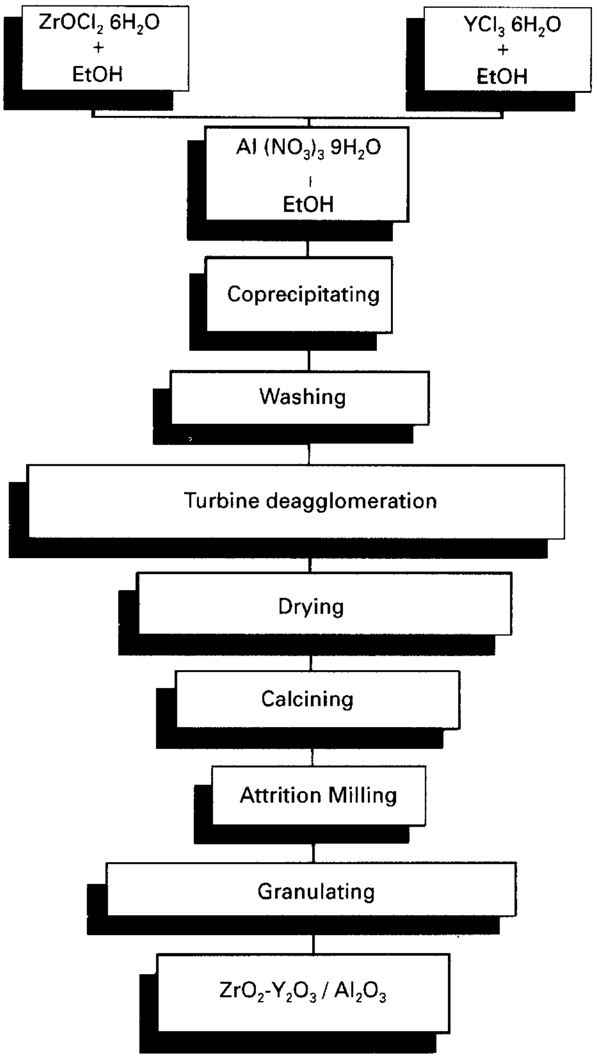

Figure 2 Flow sheet preparation of yttria-doped zirconia/Al_2O_3 composites.

Specific surface areas of both the coprecipitated and the calcined powders were determined by the BET method using N_2 as the adsorbate under high vacuum at 120 °C, and from the crystallite size calculated by X-ray diffraction [13]. Particle sizes and morphologies of the powders were estimated using TEM and SEM, with a Jeol 100CX and Carl Zeiss DSM-950, respectively.

Differential thermal analysis (DTA/TG) of the samples were made using a Netzsch STA 409 model in the temperature range 20–1000 °C, at a heating rate of 8 °C/min.

X-ray diffraction patterns of the powders were recorded using a Siemens D5000 diffractometer and filtered CuK_α radiation. Scanning rates of $2° \min^{-1}$ and $1/2° \min^{-1}$ were used for phase analysis and for crystallite size estimations respectively. Crystallite sizes were calculated by X-ray line-broadening analysis using the Scherrer equation [13].

Fourier transform infrared (FT-IR) spectroscopy was used to determine the presence of the wash solvent on the ground powders. An FT-IR spectrometer (Perkin Elmer 1760X model) with a dry air purge was used. Powder samples were mixed with dry KBr and the FT-IR cell purged for 20 min prior to spectral collection. The measurements' precision was 4 cm^{-1} and 10 scans were recorded for each sample.

3. Experimental results

3.1. Powder characterization

Fig. 3 illustrates the differential thermal analysis (DTA/TG) of the alumina gel. The curve shows a broad endothermal effect at about 250 °C and another one at 330 to 480 °C. The first corresponds to the bayerite ($Al(OH)_3$) decomposition, and the second to the decomposition of bohemite. A third endothermal effect, at about 120 °C, coincides with the lost of adsorbed water. These results, along with those obtained by X-ray diffraction, showed that above 500 °C and up to 1200 °C the only phase present was γ-alumina. As shown in the TEM photograph of Fig. 4, the particle size of alumina gel calcined at 800 °C was about 4 nm.

When the commercial zirconia was mixed with alumina gel and calcined at 800 °C, the zirconia particles appeared embedded by the smaller alumina ones, and the zirconia particle size diminished as the alumina content increased. The characteristics of the different calcined zirconia powders are shown in Table I, and the TEM photographs of Fig. 5a and b show that nanometric alumina particles of ~ 4–6 nm are finely dispersed in sub-micrometre zirconia particles of about 0.05 μm.

It must be mentioned that the presence of alumina increased the specific surface of the zirconia calcined powders, and this trend was present in all commercial zirconia–alumina series. On the other hand, it was also observed that there was a big difference between the particle size measured by TEM and that calculated from the specific surface data using the expression $D = 6/\rho\ S_{BET}$ (D is particle size, ρ is the true density and S_{BET} is the specific surface of the calcined zirconia–alumina powder). Such a particle size difference is a consequence of the powder agglomeration state and, as shown in Fig. 6 for Z-8Y samples containing 0 to 20 wt % Al_2O_3, the SEM photograph gives clear evidence of this feature. Therefore, the difference in particle size obtained by both techniques can give an idea of the zirconia powder agglomeration.

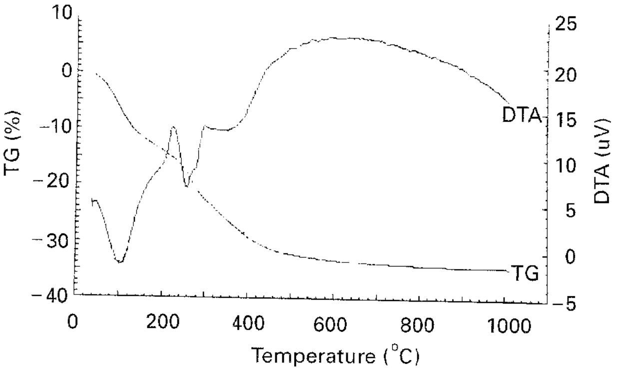

Figure 3 TG/DTA curves of alumina gel.

Fig. 7 shows the DTA curves for Z-3Y coprecipitated zirconia–yttria series without and with alumina. Two exothermic peaks are present in all the cases; the first corresponds to the combustion of the residual alcohol, and the second to the crystallization of zirconia. It must be mentioned that the alumina additions retarded the zirconia crystallization process and, as shown in the figure, the crystallization temperature for zirconia was deplaced from about 480 °C for the alumina-free zirconia sample to 780 °C for the zirconia sample containing 10 wt % alumina.

TABLE I Particle size and surface area of the different commercial calcined zirconia powders

Sample	Diameter 50% vol. Coulter (μm)	Particle size MET (nm)(a)	Specific surface (m^2/g)	Particle size (BET) (nm)
Z-8Y	0.599	38 (29)	14.2	70.6
Z-8Y/5A	0.881	37	20.1	50.9
Z-8Y/10A	0.738	35	24.6	42.6
Z-8Y-20A	0.829	30	39.8	27.6
Z-6Y	0.804	29 (34)	15.0	66.1
Z-6Y/5A	0.815	24	18.0	56.5
Z-6Y/10A	0.830	21	21.0	49.6
Z-6Y/20A	1.068	16	33.4	32.8
Z-4Y	0.979	35 (41)	18.1	54.3
Z-4Y/5A	0.671	34	20.0	50.5
Z-4Y/10A	0.630	28	27.4	37.8
Z-4Y/20A	0.748	27	38.6	28.2
Z-3Y	0.741	36 (41)	13.6	72.1
Z-3Y/5A	0.822	32	18.4	54.7
Z-3Y/10A	0.793	29	23.9	43.2
Z-3Y/20A	0.757	20	28.5	38.1

(a) In parentheses is the particle size estimated from X-ray line broadening.

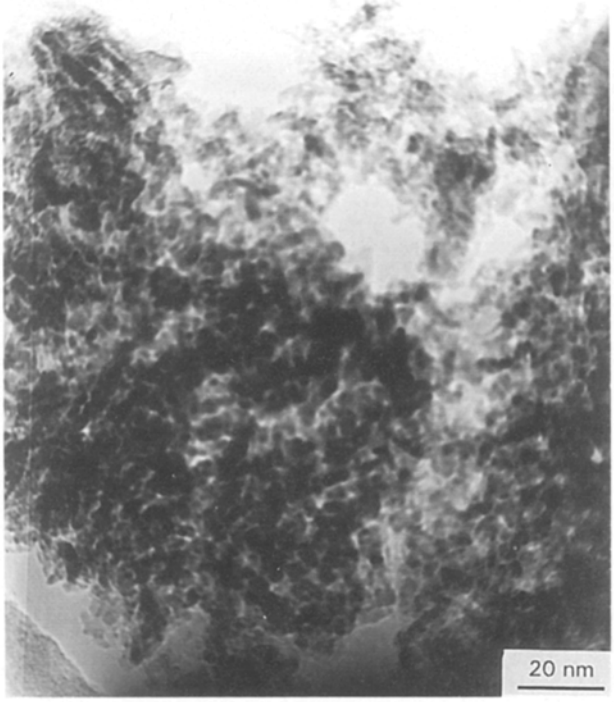

Figure 4 TEM of calcined alumina gel.

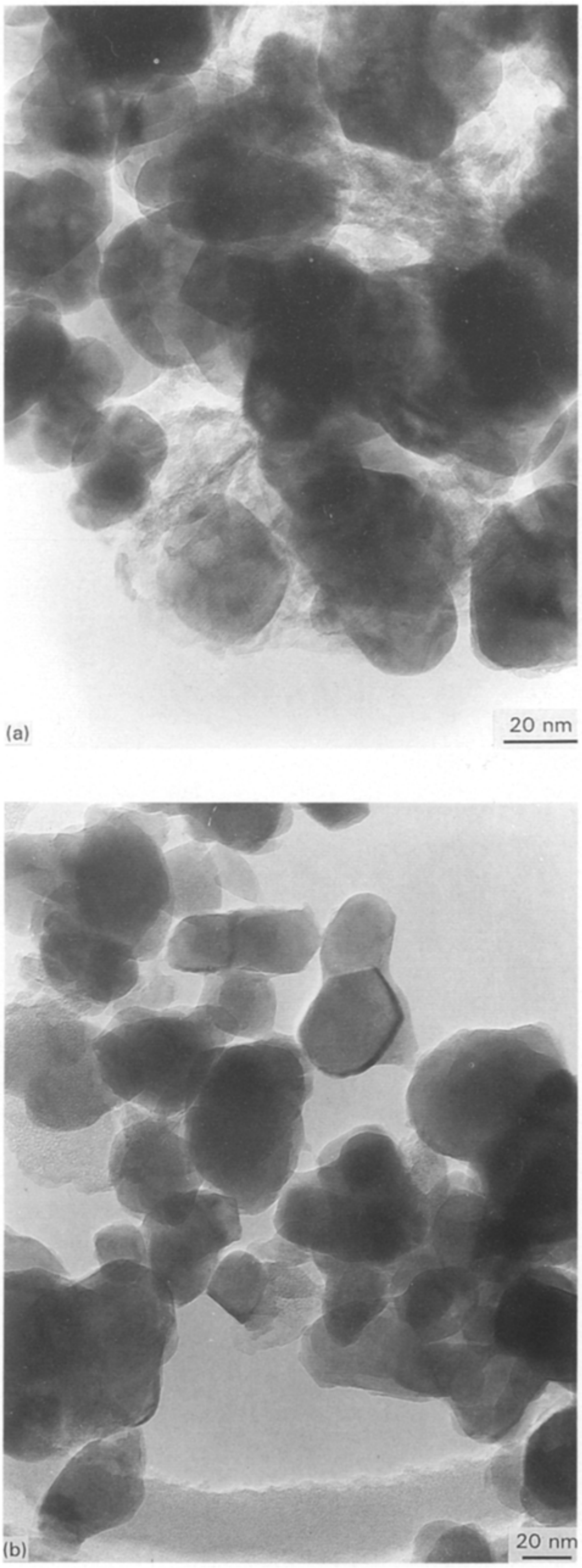

Figure 5 TEM of commercial (a) Z-3Y/10A and (b) Z-8Y/20A calcined composites.

As shown in Fig. 8, from the X-ray diffraction patterns of Z-8Y samples calcined at 300–600 °C, no crystalline phase was present for the gel or for the powder calcined at 400 °C, whereas for calcination at 600 °C the cubic phase shows up. Similar results were observed for the other alumina-free zirconia samples.

The same figure shows the X-ray diffraction patterns of the Z-8Y/10A calcined at 600 °C, 700 °C, and 800 °C for 10 minutes. The crystalline cubic zirconia phase is completely developed only at 800 °C, and for this reason all the zirconia samples with and without alumina were calcined at this temperature before sintering.

The microstructure of the calcined powders was further examined with TEM, as shown in Fig. 9, for the alumina-free Z-8Y coprecipitated zirconia sample calcined at 800 °C and with 10 wt % alumina. The particle size lies in the range of 10–20 nm and, as shown in the SEM photographs of Fig. 10a and b, some degree of agglomeration exists in the calcined powders, and it seems that the particle size for the alumina-free zirconia sample is larger than that of zirconia with 10 wt % alumina. Table II shows the main characteristics of several coprecipitated zirconia–yttria and calcined samples without and with 10 wt % alumina. As in the case of the commercial zirconia–yttria/Al_2O_3 samples, here also the addition of alumina to zirconia–yttria coprecipitated samples decreased the zirconia particle size.

3.2. Infrared spectroscopy studies

The FT-IR spectra shown in Fig. 11 correspond to the two coprecipitated zirconia powders (a) Z-8Y and (b) Z-8Y/10A. The sharp absorption bands in both spectra at ~ 1640 cm^{-1} and 3470 cm^{-1} are due to molecular water and a 0-H stretch. The two broad peaks centred at ~ 1375 and 1550 cm^{-1} seem to correspond to CO_2 adsorbed on the surface powder. The weak absorption bands at ~ 2900 to 3000 cm^{-1} are due to C-H stretching and, finally, the weak absorption bands below 1000 cm^{-1} show evidence of an interaction between isopropyl alcohol and the coprecipitated powder.

The numerical analysis by Gaussian deconvolution of the two spectra in the region of 400 to 1300 cm^{-1}, as shown in Fig. 12a and b, showed no clear evidence for the appearance of absorption bands due to Al-O stretching. However, a clear displacement of the absorption bands due to Zr-O stretching and a certain broadening of the same was evident.

4. Discussion

The above experimental results enable us to put forward some considerations on the role of alumina in the behaviour of yttria-doped zirconia powders, both these prepared by mechanically mixing ZrO_2–Y_2O_3 powder with alumina gel, and homogeneously and chemically mixed ZrO_2–Y_2O_3–Al_2O_3 powders containing 0 to 20 wt % alumina.

From the TEM photograph (Fig. 4) of the starting alumina gel dried and calcined at 800 °C, it was found that the precipitated powder was formed by very fine particles amorphous to X-ray diffraction. The calcined alumina powder was constituted by enlarged and porous particles. These particles were identified to be γ-alumina of about 4–6 nm by X-ray diffraction. The specific surface decreased from ~ 270 m^2g^{-1} in the

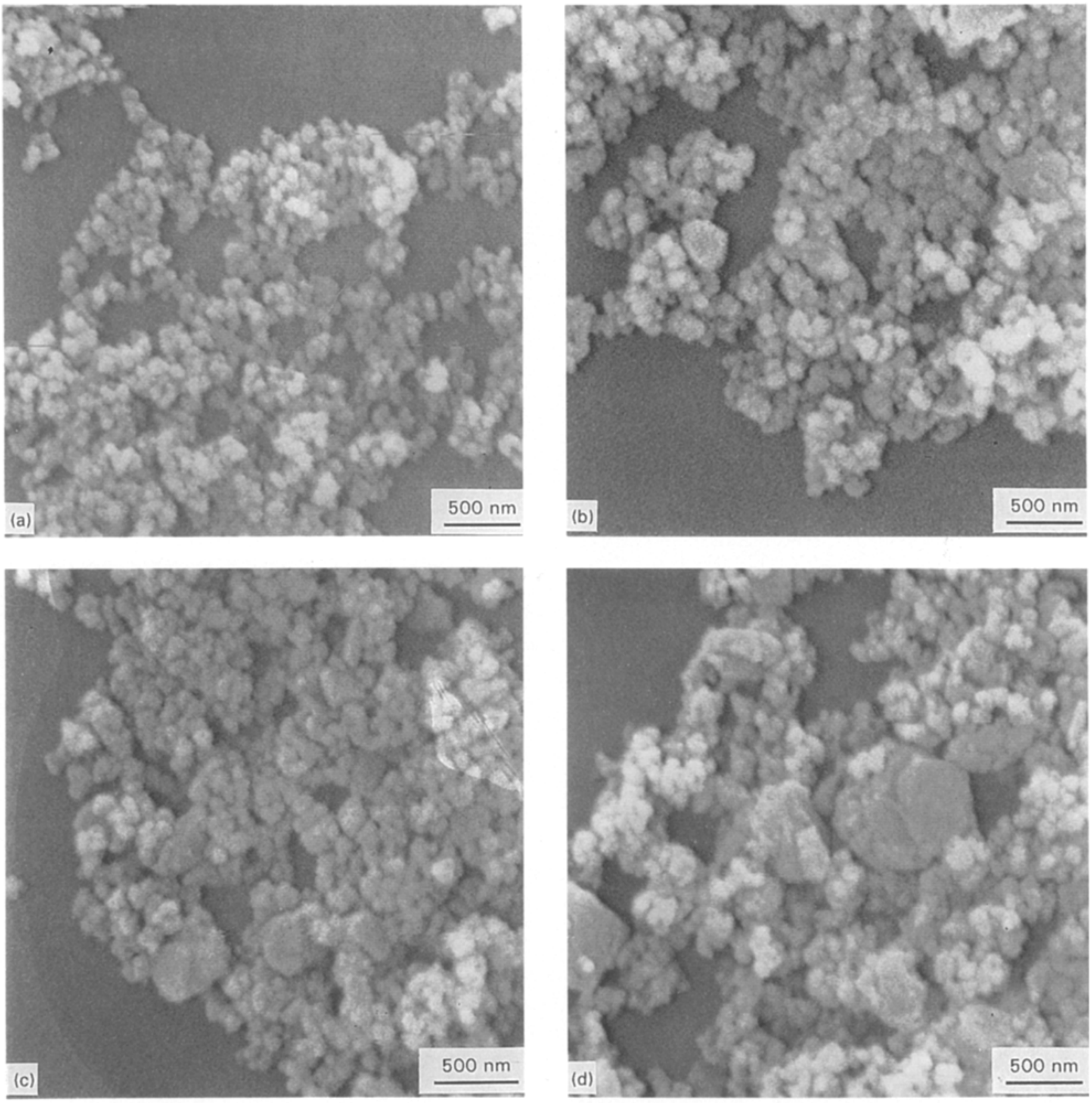

Figure 6 SEM of commercial (a) Z-8Y, (b) Z-8Y/5A, (c) Z-8Y/10A and (d) Z-8Y/20A calcined powders.

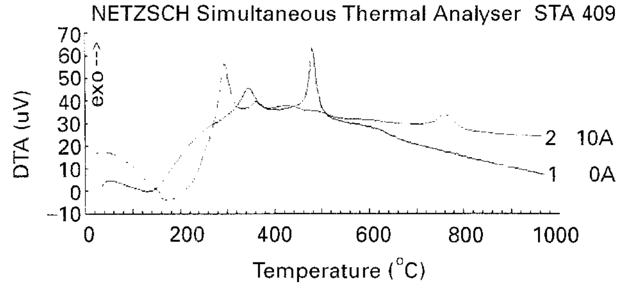

Figure 7 DTA of Z-3Y and Z-3Y/10A coprecipitated samples (NETZSCH Simultaneous Thermal Analyser STA 409).

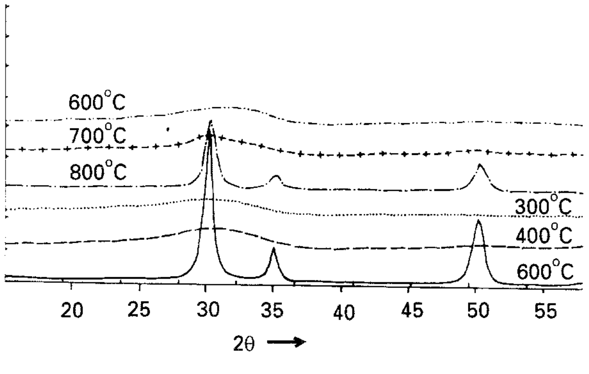

Figure 8 X-ray diffraction patterns of Z-8Y coprecipitated samples without and with 10 wt % Al_2O_3 calcined at different temperatures. The samples with 10 wt % Al_2O_3 are indicated by the −··−··, − + − + and −·−· lines.

precipitated alumina to 190 m^2g^{-1} in the γ-alumina powder.

The controlled precipitation of $Al(NO_3)_3$ in a dispersion of ZrO_2–Y_2O_3 commercial zirconia powder in anhydrous ethanol led to a two-phase powder in which the zirconia particles were encapsulated by agglomerates of $Al(OH)_3$ particles [14]. After calcining, the zirconia particles were surrounded by ultrafine γ-alumina particles; see Fig. 5. It was noticed that the zirconia particle size decreased as the alumina content increased from 35 nm in the alumina-free Z-3Y sample

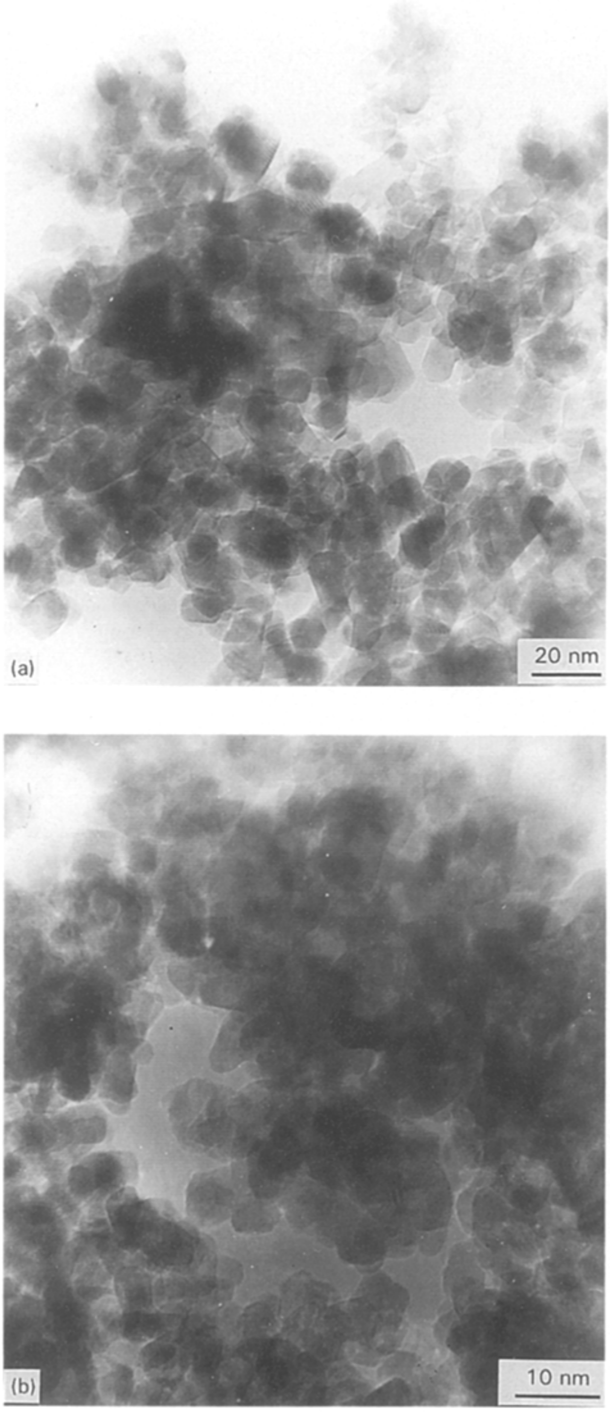

Figure 9 TEM of coprecipitated (a) Z-8Y and (b) Z-8Y/10A calcined powders.

to 20 nm in the Z-3Y/20A sample. In the same way the specific surface increased with the alumina content. Thus in the case of the Z-8Y samples it was 14 m^2g^{-1}, and 40 m^2g^{-1} for the Z-8Y/20A sample; see Table I. It could be said that by controlling the precipitation of aluminium nitrate in a zirconia powder dispersion, the production of a compositionally homogeneous two-phase zirconia–alumina oxide powder may be achieved. Such an assumption was corroborated by the observation of the calcined mixed powder by SEM (see Fig. 6), in which the relatively agglomerated zirconia powder was embedded in ultrafine alumina particles.

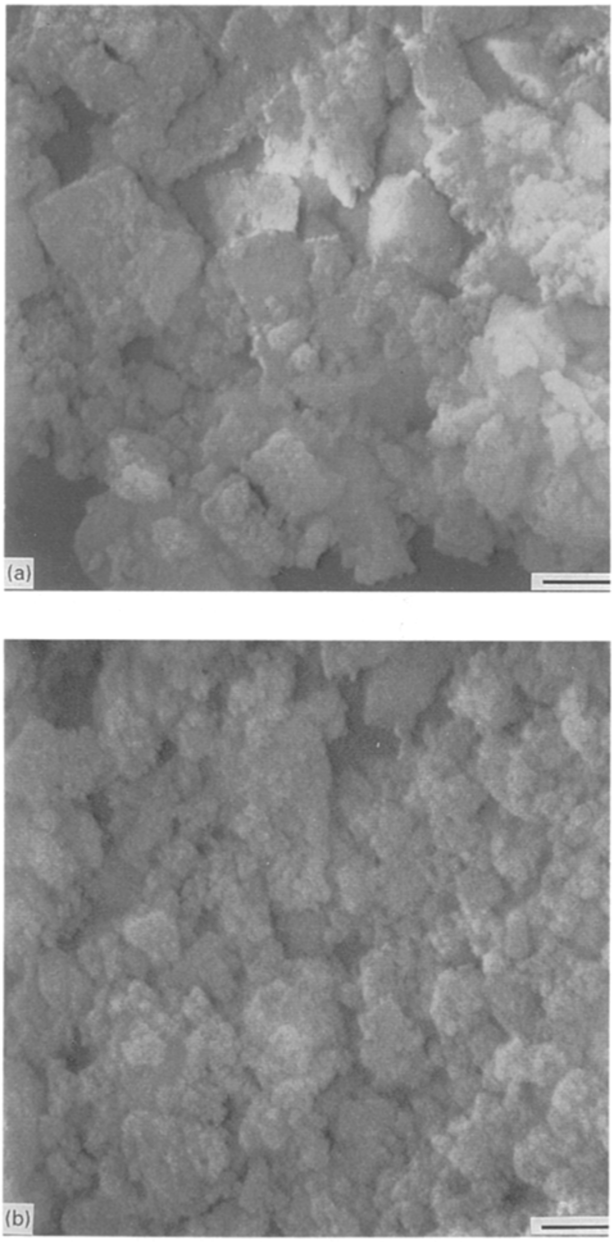

Figure 10 SEM of coprecipitated (a) Z-8Y and (b) Z-8Y/10A calcined powders (bar = 1 μm).

TABLE II Particle size and surface areas (1) coprecipitated, (2) calcined of some coprecipitated zirconia powders

Sample	Particle size (MET) (nm)(a)	Specific surface (m^2/g)(1)	Specific surface (m^2/g)(2)	Particle size (BET) (nm)
Z-8Y	8 (16)	246	53.0	18.8
Z-8Y/10A	6	205	62.0	16.9
Z-6Y	8 (16)	294	59.6	16.6
Z-6Y/10A	6	346	64.4	16.2
Z-4Y	8 (14)	285	51.0	19.3
Z-4Y/10A	5	283	65.3	15.9

(a) In parentheses is the particle size estimated from X-ray line broadening.

In the case of the well-controlled coprecipitation of Zr–Y–Al hydroxides, a chemically homogeneous coprecipitate, apparently without chlorides, was obtained. From the DTA and XRD studies (see Figs 7 and 8), it was observed that the presence of alumina

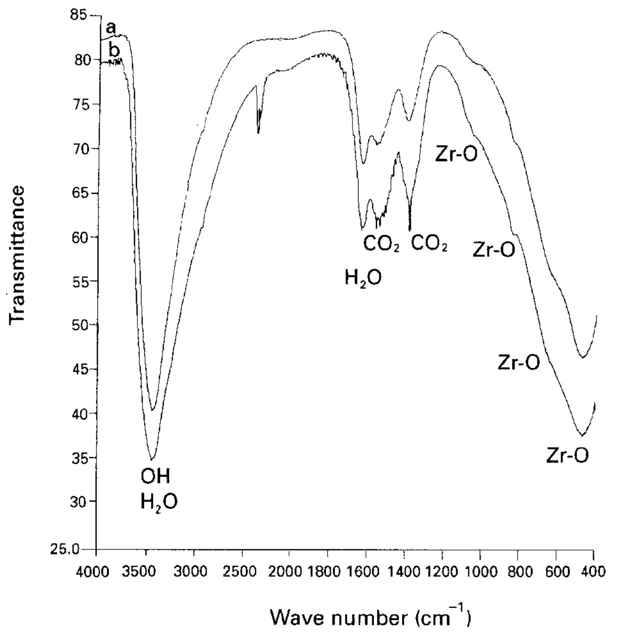

Figure 11 FT-IR spectra of coprecipitated (a) Z-8Y and (b) Z-8Y/10A powders.

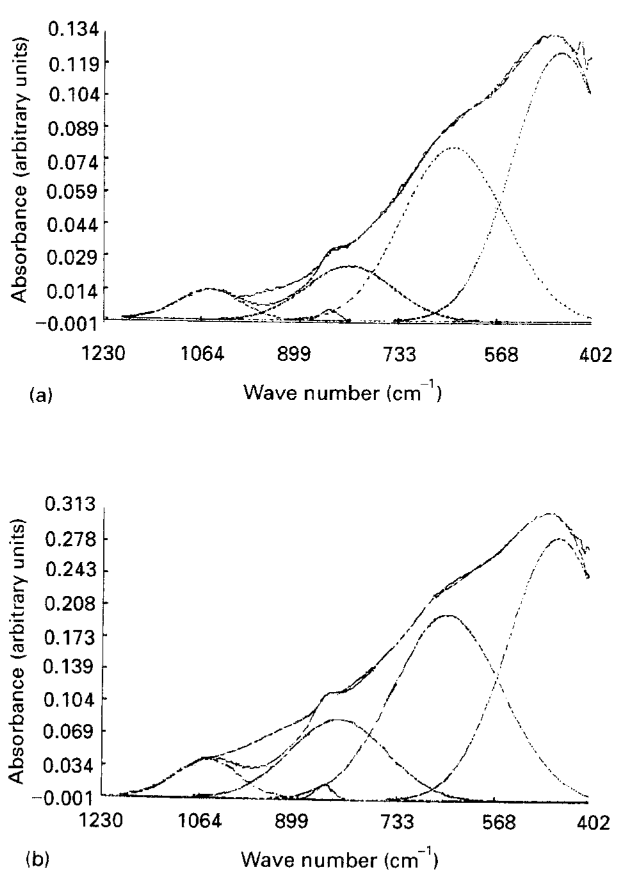

Figure 12 Gaussian deconvolution of FT-IR spectra of (a) Z-8Y and (b) Z-8Y/10A coprecipitated powders.

retarded the crystallization of zirconia. Thus the formation of relatively well-crystallized zirconia solid solution in alumina-free zirconia took place at about 600 °C, whereas in the sample containing 10 wt % Al_2O_3 such a crystallization was not produced up to about 800 °C.

The influence of alumina in retarding the crystallization zirconia temperature could be explained if it is assumed that, during the coprecipitation process, a homogeneous coprecipitate of the three hydroxides, $Zr(OH)_4 \cdot xH_2O + Y(OH)_3 \cdot yH_2O + Al(OH)_3 \cdot zH_2O$, indistinguishable by TEM, was formed. In the first step of the heat treatment, and simultaneously with the hydration water loss, a polycondensation reaction takes place with the formation of the following polycondensed chain:

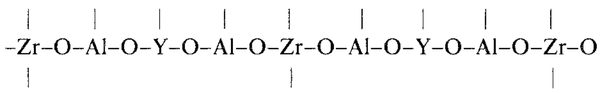

$$\text{-Zr-O-Al-O-Y-O-Al-O-Zr-O-Al-O-Y-O-Al-O-Zr-O}$$

If this is so, then the interdiffusion distances will be much longer than those of the -Zr-O-Y-O-Zr- condensed chain. In such a situation it seems probable that some Al^{3+} cations will be incorporated into the ZrO_2 particles surface, impeding, thus, the access of Y^{3+} cations to the zirconia matrix and, at the same time, retarding its crystallization. This interpretation is supported by the IR spectra shown in Figs 11 and 12. According to these results it seems evident that $Al(OH)_3$ particles are not like discrete ones in the whole of the Y-Zr-Al coprecipitate, but intercalated between the Zr-O groups giving rise to a higher disordering level or a higher amorphization of the coprecipitate. The fact of some displacement of the absorption bands due to Zr-O stretching, and non-appearance of well-located absorption bands due to Al-O stretching, support that idea. On the other hand, the TEM of Fig. 9 shows that the zirconia particles, the dark areas, are coated by ultrafine alumina particles, the less dark areas. Fegley *et al.* [15] and Murase *et al.* [16] reported that a similar phenomenon occurred during the controlled hydrolysis of a zirconium alkoxide or $Al(NO_3)_3$ in a dispersion of α-alumina or zirconia powders, respectively. In this case a film of zirconia coated the alumina particles or monoclinic zirconia coated by ultrafine alumina particles, respectively, took place. On the other hand, Rajendran *et al.* [17] assumed that both Zr^{4+} and Al^{3+} were uniformly distributed in an amorphous powder which, as the temperature increased, controlled the diffusion of Zr^{4+} and Y^{3+}. In our case we assume that some Al^{3+} cations interact with the zirconia matrix [18], forming a thin film grain boundary which acts as a barrier to the diffusion of the Y^{3+} cations. At higher temperatures the reaction-rate of ZrO_2 with Y_2O_3 is much higher than that of ZrO_2 with alumina. Therefore, knowledge of the higher temperature phenomena could contribute to clarifying the role of alumina in zirconia powder processing.

A complete investigation of the sintering behaviour and microstructural development of these compacted powders will be presented in a forthcoming paper [19].

Acknowledgements

This work was supported by the European Commission under contract JOUE-044-C. Special thanks go to J. Rubio for his help with the FT-IR experiments.

References

1. E. BAUER and H. PREIS, *Z. Elektrochem.* **43** (1937) 727.
2. L. G. J. de HAART and K. J. de VRIES, in "Multichannel solid oxide fuel reactors", EN3E/0167E CEC Research Project, Final Report (1989) p. 36.
3. B. Q. MINH, *J. Am. Ceram. Soc.* **76** (1993) 563.
4. M. RUHLE, N. CLAUSSEN and A. H. HEUER, in "Advances in ceramics", Vol. 12, Science and Technology of Zirconia II, edited by N. Claussen, M. Ruhle and A. H. Heuer (Amer. Ceram. Soc., Columbus, OH, 1984) pp. 352–70.
5. A. D. KULJARNI, C. D. JOHNSON, and G. W. PERBIX, *J. Inst. Metals* **99** (1971) 15.
6. T. H. ETSELL and S. N. FLENGAS, *Chem Rev.* **70** (1970) 339.
7. T. TAKAHASHI and A. KOZAWA, "Applications of solid electrolytes" (JED Press, Tokyo, 1980).
8. F. K. MAGHADAM and D. A. STEVENSON, *J. Am. Ceram. Soc.* **66** (1982) 213.
9. T. K. GUPTA, J. H. BETCHOLD, R. C. KUZNICKI, L. H. CADOFF and B. R. ROSSING, *J. Mater. Sci.* **12** (1977) 2421.
10. E. P. BUTLER and A. H. HEUER, *J. Am. Ceram. Soc.* **68** (1985) 197.
11. S. P. S. BADWAL, *J. Mater. Sci.* **18** (1983) 3230.
12. F. J. ESPER, K. H. FRIESE and H. GEIER, *Advances in Ceramics* **12** (1982) 528.
13. K. D. KLUG and L. E. ALEXANDER, "X-ray diffraction procedures" (Wiley, New York, 1974) pp. 618–708.
14. L. M. NAVARRO, PhD thesis, Alcalá de Henares University, Madrid (1994).
15. B. FEGLEY Jr., P. WHITE and H. K. BOWEN, *J. Am. Ceram. Soc.* **68** (1985) C-60.
16. Y. MURASE, E. KATO and K. DAIMON, *J. Am. Ceram. Soc.* **69** (1986) 83.
17. S. RAJENDRAN, H. J. TOSSELL and J. V. SANDERS, *J. Mater. Sci.* **24** (1989) 1195.
18. J. BANNISTER, *J. Aust. Ceram. Soc.* **18** (1982) 6.
19. L. M. NAVARRO, P. RECIO and P. DURAN, *J. Mater. Sci.* Submitted.

Received 29 July
and accepted 11 August 1994